Research Article Vol. 57, No. 33 / 20 November 2018 / Applied Optics 9777

applied optics

Moiré fringes of higher-order harmonics versus higher-order moiré patterns

Mohammad Yeganeh[1,†] and Saifollah Rasouli[1,2,*,†]

[1]Department of Physics, Institute for Advanced Studies in Basic Sciences (IASBS), Zanjan 45137-66731, Iran
[2]Optics Research Center, Institute for Advanced Studies in Basic Sciences (IASBS), Zanjan 45137-66731, Iran
*Corresponding author: rasouli@iasbs.ac.ir

Received 13 August 2018; revised 19 October 2018; accepted 19 October 2018; posted 22 October 2018 (Doc. ID 342184); published 16 November 2018

This work presents a very simple and comprehensive approach for classification of the combinational spatial frequencies of the superimposed periodic or quasi-periodic structures. The reciprocal vectors of the structures are used to express their respective spectral components, and a unique reciprocal vectors equation is introduced for presenting the corresponding combinational frequencies. By the aid of the reciprocal vectors equation we classify moiré patterns of combinational frequencies into four classes: the conventional moiré pattern, moiré fringes of higher-order harmonics, higher-order moiré patterns, and pseudo-moiré patterns. The difference between the moiré fringes of higher-order harmonics and higher-order moiré patterns is expressed in the formulas. By some typical examples, conditions for simultaneous formation of moiré patterns of different harmonics of the superimposed gratings are investigated. We show that in the superimposition of two gratings, where at least one has a varying period and another has a non-sinusoidal profile, different moiré patterns are formed over different parts of the superimposed area, where a distinct pair of spatial frequencies of the superimposed structures contributes to the formation of each of the patterns. We use the same procedure in the analysis of simultaneously produced defected moiré patterns in the superimposition of a linear grating and a zone plate, where one or both consist of some topological defects at specific locations and at least one of the gratings has a non-sinusoidal profile. The topological defects of resulting moiré fringes are similar to those appearing in the interference patterns of optical vortices. It is shown that the defect number of resulting moiré fringes depends on the defect numbers and order of frequency harmonics of the gratings. The dependency of the defect number of the moiré fringes and its sign to the defect numbers of the gratings and their contributed frequency harmonics is derived for both additive and subtractive terms of moiré fringes, and the results are verified with several examples based on computational simulations.

https://doi.org/10.1364/AO.57.009777

1. INTRODUCTION

Periodic structures known as gratings, rulings, or grids have many applications in different branches of optics. Vasco Ronchi is the pioneer in manufacturing and use of gratings or rulings [1]. Gratings or rulings with spatial periods in a range of micrometers to centimeters have found various applications in optics ranging from the spectroscopy to the amateur telescope making. Another application of the gratings is in the moiré technique. In general, when two periodic or semi-periodic structures are superimposed, a new periodic structure with a larger spatial period appears that is well known as the moiré pattern. During the past four decades, the moiré technique in different arrangements has been well established as a simple and powerful means for different measurements in physics and engineering. In parallel to the advent of various applications for the moiré technique, its formulation has also been developed and different methods have been proposed for investigating moiré patterns [2–9].

In most applications, moiré fringes form with the contribution of first-order or fundamental frequencies of the superimposed structures. In this case, the values of periods of the superimposed structures are close. Moiré fringes of higher-order frequencies are produced when higher harmonics of the superimposed structures make appreciable contributions in the resulting pattern. The use of moiré fringes of higher-order frequencies exhibits enhanced sensitivity [10]. For instance, moiré fringes of higher-order frequencies were recently used in a nano-moiré atomic force microscope (AFM) for increasing the sensitivity of the in-plane displacements. Its work is based on the spatial beating effect between the mth harmonic of a non-sinusoidal profile quasi-periodic specimen and the first harmonic of a reference grating [11]. In both cases,

resulting low-frequency fringes are known as the first-order moiré pattern. On the other hand, in the superimposition of two gratings, higher-order moiré patterns can be obtained by filtering the first-order moiré fringes from the resulting superimposed pattern. The higher-order moiré fringes are contributed on the profile of the resulting moiré pattern in which by removing all the higher-order moiré fringes the profile of the first-order moiré fringes will be a sinusoidal form.

Let us explain the difference between "higher-order moiré fringes" and "moiré fringes of higher-order frequencies" by an example. Consider a moiré pattern of two gratings with the same periods and having non-sinusoidal profiles. In this case a first-order moiré pattern forms by contribution of fundamental frequencies of the superimposed gratings and a higher-order moiré pattern is formed by the contribution of a pair of higher-order frequencies of the gratings having equal values. In practice, the intensity of the higher-order moiré fringes is insignificant, such that only the lowest-order moiré fringes are readily observed. The spatial period of a higher-order moiré pattern with an order of n is $\frac{1}{n}$ times of the period of the first-order moiré pattern. By removing impulses of the lowest-order moiré patterns in the frequency domain, one can improve visibility of a higher-order moiré pattern.

In a former study with the aid of parametric equations, formulation of moiré patterns of higher-order frequencies is presented [12]. In the parametric equations method, a moiré fringe is only determined by its trace equation. Therefore, there is no continuous information over the fringes pattern and consequently this method suffers from the low spatial resolution. In two recent works moiré patterns of higher orders are used for different purposes [13,14].

We have recently introduced a simple method for the study of moiré patterns of gratings having sinusoidal profiles by using the reciprocal vectors approach [15,16]. This method can be used for presenting a variety of periodic or quasi-periodic structures having topological defects and predicting behavior of their moiré patterns [17,18]. A grating with a sinusoidal transmission profile has three spatial frequency components, consisting of the dc or the zero order and plus and minus first orders. Therefore, in the superimposition of two gratings with sinusoidal profiles, only first-order moiré patterns of fundamental frequencies are detectable. In this work, we take into account higher-order spatial frequency components of the superimposed gratings, when at least one of them has a varying period, and investigate simultaneous formation of moiré patterns of different harmonics of the gratings by the aid of the reciprocal vectors equation. A grating having a binary profile with a given value of opening number (sometimes called filling factor of the grating) or a grating with a three-level transmission value are typical examples of the gratings that have higher-order spatial frequencies in their spatial spectra or equally in their Fourier expansions [19]. For instance, a Ronchi ruling has a two-level or binary transmission profile with an opening number of $\frac{1}{2}$, and it has only odd orders of spatial frequencies in the spectrum. As in the reciprocal vectors approach a continuous phase function is assigned to each of the superimposed gratings and also to the resulting moiré pattern, measured physical quantities such as characteristics of the superimposed gratings can be determined from the moiré pattern over the entire superimposed area.

In this work using the reciprocal vectors equation approach, a comprehensive formulation for moiré fringes of higher-order harmonics and higher-order moiré patterns is presented, and the difference of moiré fringes of higher-order harmonics with higher-order moiré patterns is expressed. By the aid of the presented formulation, moiré patterns of different higher-order frequencies of a linear grating consisting of topological defects with a Fresnel zone plate are investigated. We show that the defect of the defected grating is magnified by the resulting moiré fringes in which the defect number of the resulting moiré fringes is equal to the product of defect number of the defected grating and order number of the contributed frequencies in the moiré pattern. Also, superimposition of the defected linear grating and defected zone plate is investigated with more details.

Furthermore, in this work we use the reciprocal vectors equation approach for presenting pseudo-moiré, in which it appears as a modulation effect and having no corresponding impulses in the Fourier spectral domain [20].

2. BASIC CONCEPTS OF THE RECIPROCAL VECTOR EQUATION APPROACH

The transmission function of a grating can be written as

$$t(\boldsymbol{\rho}) = \sum_{m=-\infty}^{\infty} c_m \exp[im\phi(\boldsymbol{\rho})], \tag{1}$$

where $\phi(\boldsymbol{\rho})$ is the phase function of the grating and $\boldsymbol{\rho}$ is the position vector over the grating. c_ms are expansion coefficients and define the grating type; for example, for a sinusoidal grating only $m = 0, \pm 1$ exist. The spectrum of the spatial frequencies shows all frequency components of the transmission function, and can be written as

$$T(\mathbf{G}) = \sum_{m=-\infty}^{\infty} C_m \delta[\mathbf{G} - m\nabla\phi(\boldsymbol{\rho})], \tag{2}$$

where δ is the Dirac delta function and $\nabla\phi(\boldsymbol{\rho}) = \mathbf{G}^{(1)}(\boldsymbol{\rho})$ is the local reciprocal vector of the grating and its value $|\mathbf{G}^{(1)}(\boldsymbol{\rho})|$ shows the fundamental frequency of the grating at position $\boldsymbol{\rho}$. By considering Eq. (1) and using following equation [16]:

$$\mathbf{G}^{(m)}(\boldsymbol{\rho}) = -i\frac{\nabla t^{(m)}(\boldsymbol{\rho})}{t^{(m)}(\boldsymbol{\rho})}, \qquad m \in \mathbb{Z}, \tag{3}$$

one can calculate the mth component of the spatial frequency of the grating at the vicinity of the position $\boldsymbol{\rho}$, where $t^{(m)}(\boldsymbol{\rho})$ is the mth term of Eq. (1). From Eqs. (1) and (3), the mth-order component of the grating's local frequency is obviously m times of the fundamental local frequency of the grating:

$$\mathbf{G}^{(m)}(\boldsymbol{\rho}) = m\mathbf{G}^{(1)}(\boldsymbol{\rho}), \qquad m \in \mathbb{Z}. \tag{4}$$

In the superimposition of two gratings having transmission functions of $t_1(\boldsymbol{\rho})$ and $t_2(\boldsymbol{\rho})$, the resulting transmission function in the space and spatial frequency domains are, respectively,

$$t_{\text{res}}(\boldsymbol{\rho}) = \sum_{m_1, m_2=-\infty}^{\infty} c_{m_1} c_{m_2} \exp[im_1\phi_1(\boldsymbol{\rho})] \exp[im_2\phi_2(\boldsymbol{\rho})], \tag{5}$$

$$T_{\text{res}}(\mathbf{G}) = \sum_{m_1, m_2 = -\infty}^{\infty} C_{m_1} C_{m_2} \delta[\mathbf{G} - m_1 \mathbf{G}_1(\boldsymbol{\rho}) - m_2 \mathbf{G}_2(\boldsymbol{\rho})], \quad (6)$$

where indices 1 and 2 refer to the first and second gratings and for both of the equations $m_1, m_2 \in \mathbb{Z}$. Transmitted light containing a set of spatial frequencies is given by the following equation:

$$\mathbf{G} = m_1 \mathbf{G}_1^{(1)} + m_2 \mathbf{G}_2^{(1)}, \qquad m_1, m_2 \in \mathbb{Z}, \quad (7)$$

where $\mathbf{G}_1^{(1)}$ and $\mathbf{G}_2^{(1)}$ are the fundamental frequencies of the gratings.

In Fig. 1(a) two similar binary (no Ronchi) gratings having a small angle between their lines and a period Λ_0 are illustrated. In Fig. 1(d) two binary (no Ronchi) gratings with periods $\Lambda_1 = 2\Lambda_0$ and $\Lambda_2 = 3\Lambda_0$ again having the same small angle between their lines are shown. Dependency of $\mathbf{G}$ to the local period of the grating is given by $\mathbf{G}(\boldsymbol{\rho}) = \frac{2\pi}{\Lambda(\boldsymbol{\rho})}\hat{G}$, in which $\hat{G}$ is a unit vector perpendicular to the lines of the grating. In practice the angle between the lines of the gratings is less than several degrees.

In Figs. 1(b) and 1(e) the fundamental frequencies of the gratings, $\mathbf{G}_1^{(1)}$ and $\mathbf{G}_2^{(1)}$, and their higher harmonics, $\mathbf{G}_1^{(2)}$, $\mathbf{G}_1^{(3)}, \ldots$ and $\mathbf{G}_2^{(2)}, \mathbf{G}_2^{(3)}, \ldots$, are shown by point impulses.

Figure 1(c) shows, from the left to right, the resulting pattern of superimposition of the gratings shown in Fig. 1(a), respective conventional moiré fringes, and second-order moiré fringes. For the case of two gratings introduced in Fig. 1(d), the resulting superimposed pattern, the corresponding first-order moiré fringes and second-order moiré fringes are illustrated in Fig. 1(f) from the left to right, respectively. As can be deduced, and also will be discussed below, here the first-order moiré pattern, $\mathbf{G}_{\text{moire}'}^{(1)}$, forms by contribution of frequency components of $(\pm\mathbf{G}_1^{(2)}, \pm\mathbf{G}_2^{(3)})$, and the next lowest frequency components of $(\mathbf{G}_1^{(4)} = 2\mathbf{G}_1^{(2)}, \mathbf{G}_2^{(6)} = 2\mathbf{G}_2^{(3)})$ are responsible to make the second-order moiré fringes, $\mathbf{G}_{\text{moire}'}^{(2)}$. In fact, the second-order moiré pattern is almost hidden behind the original moiré pattern and after removing impulses of the first-order moiré pattern its pattern appears remarkably. Below, by details we determine the difference of moiré patterns of higher-order harmonics and higher-order moiré patterns.

It is worth noting that Figs. 1(b) and 1(e) show the respective spectra of the individual gratings and they do not show the respective spectrum of the superimposition of the gratings. Therefore, it differs with the moiré patterns' spectra were

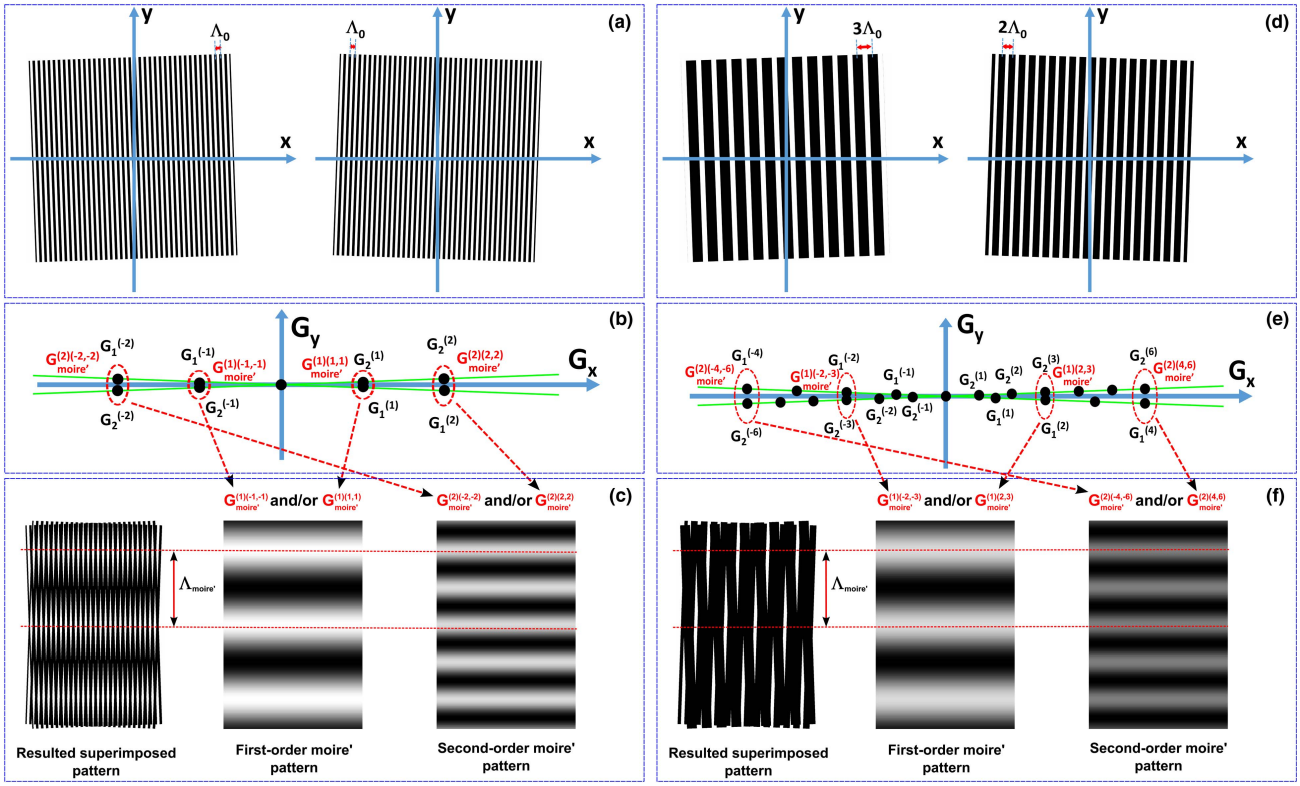

Fig. 1. (a) Two binary (no Ronchi) gratings with the same period Λ_0 with a small angle between their lines. (b) Illustration of frequency components of the gratings in the frequency domain (it does not illustrate the respective spectrum of the resulting moiré pattern). Two pairs of the frequency components $\mathbf{G}_1^{(1)}$ and $\mathbf{G}_2^{(1)}$ make first-order moiré fringes (the conventional moiré fringes) and two other pairs $\mathbf{G}_1^{(2)}$ and $\mathbf{G}_2^{(2)}$ responsible to make second-order moiré fringes. (c) From left to right, the resulting pattern of superimposition of the gratings, respective conventional moiré fringes, and second-order moiré fringes. (d) Two typical binary (no Ronchi) gratings with periods $\Lambda_1 = 2\Lambda_0$ and $\Lambda_2 = 3\Lambda_0$ with a small angle between their lines. (e) Illustration of frequency components of the gratings in the frequency domain. In this case, two pairs of the frequency components $\mathbf{G}_1^{(2)}$ and $\mathbf{G}_2^{(3)}$ make first-order moiré fringes and two other pairs $\mathbf{G}_1^{(4)}$ and $\mathbf{G}_2^{(6)}$ are responsible to make second-order moiré fringes. (f) From left to right, the resulting superimposed pattern, respective first-order moiré fringes, and second-order moiré fringes. When the higher-order frequencies contribute in the formation of moiré fringes, their contrast decreases.

usually used in the spectral approach, such as in [9]. However, each of the impulses of a given moiré pattern's spectrum can be produced by a suitable combination of the different harmonics of the superimposed structures using Eq. (7).

In the next section using the reciprocal vectors equation approach, we present a comprehensive classification of combinational frequencies of higher spectral components of two superimposed periodic or quasi-periodic structures. This approach can be also applied on three or more gratings placed together. We classify the combinational frequencies of the superimposed structures into four classes: the conventional moiré pattern, the moiré fringes of higher-order harmonics, the higher-order moiré patterns, and pseudo-moiré patterns. It is worth noting that some aspects of the proposed classification in practice were used in minimization of the moiré effect in the display devices [21,22].

3. MOIRÉ FRINGES OF HIGHER-ORDER HARMONICS AND HIGHER-ORDER MOIRÉ PATTERNS

Here we define moiré pattern, determine conditions of formation of a moiré pattern, and consider different moiré patterns of superimposition of two periodic structures. Also, conventional or first-order moiré patterns, including moiré fringes of fundamental and higher-order harmonics of the gratings and higher-order moiré patterns, are defined by the aid of the reciprocal vectors equation.

- **The moiré pattern** is determined by the minimum value of $\mathbf{G}$ in Eq. (7) obtained with any combination of m_1 and m_2, in which $\mathbf{G}$ is considerably smaller than both of the fundamental frequencies of the superimposed gratings.
- **The first-order moiré pattern of first-order frequencies** is formed by contribution of fundamental frequencies of the superimposed gratings. When the local pitch of the gratings is almost equal the fundamental frequencies of the gratings contribute in the formation of a moiré pattern. In this case, the reciprocal vector of the resulted moiré pattern is given by

$$\mathbf{G}_{\text{moire}'}^{(1)(1,1)} = \pm \min[(\mathbf{G}_1^{(1)} + \mathbf{G}_2^{(1)}), (\mathbf{G}_1^{(1)} - \mathbf{G}_2^{(1)})], \tag{8}$$

where, in the superscript of $\mathbf{G}_{\text{moire}'}^{(1)(1,1)}$ the number of first parentheses shows the order of moiré fringes and the second shows orders of the contributed frequencies of the gratings in the resulting moiré pattern, and the plus and minus terms refer to additive and subtractive first-order moiré fringes, respectively. We use the "min" function to show the minimum between vector norms. When direction of the reciprocal vector of one of the gratings varies over the superimposed area, the contributed term in the moiré fringes may alter between the sum and difference terms at distinct regions over the superimposed area.

As a grating with a sinusoidal transmission profile has only the dc and ± 1 orders in its Fourier expansion, in the superimposition of two sinusoidal gratings only the first-order moiré pattern can be formed.

In a case $\mathbf{G}_1^{(1)} \| \mathbf{G}_2^{(1)}$, **parallel moiré fringes** form, and when $\mathbf{G}_1^{(1)} = \mathbf{G}_2^{(1)}$, **infinite-mode moiré fringes** with a spatial frequency of zero appear.

- **A first-order moiré pattern with higher-order frequencies** is formed by contribution of at least one of the higher-order frequencies of the superimposed gratings.

As a simple example, consider that the fundamental frequency of the first grating is half of the second one, $|\mathbf{G}_2^{(1)}| = 2|\mathbf{G}_1^{(1)}|$, then the minimum value of Eq. (7) is given by $m_1 = 2$ and $m_2 = 1$, in which $|\min[(2\mathbf{G}_1^{(1)} + \mathbf{G}_2^{(1)}), (2\mathbf{G}_1^{(1)} - \mathbf{G}_2^{(1)})]| < |\min[(\mathbf{G}_1^{(1)} + \mathbf{G}_2^{(1)}), (\mathbf{G}_1^{(1)} - \mathbf{G}_2^{(1)})]|$. Here, the reciprocal vector of the resulting lowest-order moiré pattern is given by

$$\begin{aligned}\mathbf{G}_{\text{moire}'}^{(1)(2,1)} &= \pm \min[(2\mathbf{G}_1^{(1)} + \mathbf{G}_2^{(1)}), (2\mathbf{G}_1^{(1)} - \mathbf{G}_2^{(1)})] \\ &= \pm \min[(\mathbf{G}_1^{(2)} + \mathbf{G}_2^{(1)}), (\mathbf{G}_1^{(2)} - \mathbf{G}_2^{(1)})].\end{aligned} \tag{9}$$

As a more general case of first-order moiré fringes of higher-order frequencies, consider that $|m_1\mathbf{G}_1^{(1)}|$ and $|m_2\mathbf{G}_2^{(1)}|$ are almost equal, where $m_1, m_2 \in \mathbb{Z}$, and they are coprime. As the minimum value of Eq. (7) determines the moiré pattern, therefore the reciprocal vector of the resulting lowest-order moiré pattern is given by

$$\begin{aligned}\mathbf{G}_{\text{moire}'}^{(1)(m_1,m_2)} &= \pm \min[(m_1\mathbf{G}_1^{(1)} + m_2\mathbf{G}_2^{(1)}), (m_1\mathbf{G}_1^{(1)} - m_2\mathbf{G}_2^{(1)})] \\ &= \pm \min[(\mathbf{G}_1^{(m_1)} + \mathbf{G}_2^{(m_2)}), (\mathbf{G}_1^{(m_1)} - \mathbf{G}_2^{(m_2)})].\end{aligned} \tag{10}$$

Here, again, parallel moiré fringes form when $\mathbf{G}_1^{(1)} \| \mathbf{G}_2^{(1)}$, and infinite-mode moiré fringes appear if $m_1\mathbf{G}_1^{(1)} = m_2\mathbf{G}_2^{(1)}$.

Both former cases can be considered as the **lowest-order moiré pattern** that can be easily observed over the superimposed area. Below we present the **higher-order moiré pattern** in which these kinds of patterns are hidden behind the original moiré pattern.

- **The higher-order moiré pattern** is formed by the contribution of integer multiples of the gratings frequencies contributed in an existence lowest-order moiré pattern. Consider that in the formation of the lowest-order moiré pattern, higher-order frequencies of $(\mathbf{G}_1^{(m_1)} = m_1\mathbf{G}_1^{(1)}, \mathbf{G}_2^{(m_2)} = m_2\mathbf{G}_2^{(1)})$ contribute. In this case, the nth-order moiré pattern is given by

$$\begin{aligned}&\mathbf{G}_{\text{moire}'}^{(n)(nm_1,nm_2)} \\ &= \pm \min[(nm_1\mathbf{G}_1^{(1)} + nm_2\mathbf{G}_2^{(1)}), (nm_1\mathbf{G}_1^{(1)} - nm_2\mathbf{G}_2^{(1)})] \\ &= \pm \min[(n\mathbf{G}_1^{(m_1)} + n\mathbf{G}_2^{(m_2)}), (n\mathbf{G}_1^{(m_1)} - n\mathbf{G}_2^{(m_2)})],\end{aligned} \tag{11}$$

where

$$\mathbf{G}_{\text{moire}'}^{(n)(nm_1,nm_2)} = n\mathbf{G}_{\text{moire}'}^{(1)(m_1,m_2)}. \tag{12}$$

In Fig. 1(e), a case of $\mathbf{G}_{\text{moire}'}^{(2)(4,6)} = 2\mathbf{G}_{\text{moire}'}^{(1)(2,3)}$ is illustrated. As is apparent, the spatial period is divided by n in an nth-order moiré pattern but still moiré fringes have the same orientation of the first-order moiré fringes.

- When grids of the superimposed grating are parallel and $\mathbf{G}_2^{(1)} = m_1\mathbf{G}_1^{(1)}$, where m_1 is an integer, as mentioned above an infinite-mode moiré pattern with a spatial frequency of zero forms. Meanwhile, the resulting pattern still has a fine periodicity the same as the periodicity of the first grating, but the transmission profile of the resulting pattern differs from both profiles of the superimposed gratings (see Fig. 2). This behavior appears for both sinusoidal and binary gratings.

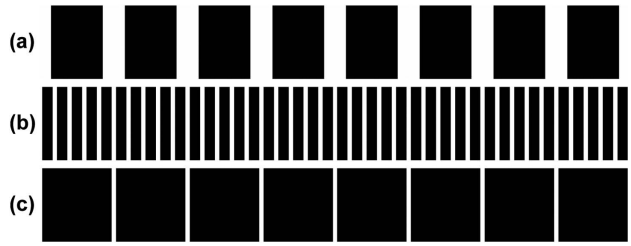

Fig. 2. Two linear binary gratings with the same opening numbers equal to 0.3 and periods: (a) $\Lambda_1 = 5\Lambda_0$ and (b) $\Lambda_2 = \Lambda_0$. (c) Resulting pseudo-moiré pattern with a period equal to Λ_1.

• When $m_1\mathbf{G}_1^{(1)} = m_2\mathbf{G}_2^{(1)}$ in which m_1 and m_2 are coprime, the period of the higher-frequency resulting pattern is equal to the *least common multiple* of the gratings' periods. As the period of the resulting pattern is several times of the periods of the superimposed gratings, it appears as a modulation effect and has no corresponding impulses in the Fourier spectral domain [20]. This pattern is known as the **pseudo-moiré pattern**. Similarly, for all cases of $|\mathbf{G}| \approx (|\mathbf{G}_1|, |\mathbf{G}_2|)$, the resulting patterns can be called pseudo-moiré patterns. Some relevant results of the pseudo-moiré can be found in [20,23,24].

4. SEVERAL EXAMPLES

In the following, several useful examples are presented.

A. First- and Higher-Order Moiré Fringes of Two Linear Binary Gratings of $\Lambda_1 = 2\Lambda_2$

Here, superimposition of two linear gratings having binary profiles with periods of $\Lambda_1 = 2\Lambda_2 = 2\Lambda_0$ is considered in which $|\mathbf{G}_2^{(1)}| = |\mathbf{G}_1^{(2)}| = 2|\mathbf{G}_1^{(1)}|$, $m_1 = 2$, and $m_2 = 1$. It is also considered that lines of the gratings have an angle of θ. In this case, fundamental frequencies of the gratings can be written as

$$\begin{aligned}\mathbf{G}_1^{(1)} &= \frac{2\pi}{2\Lambda_0}\left[\cos\left(\frac{\theta}{2}\right)\hat{x} + \sin\left(\frac{\theta}{2}\right)\hat{y}\right],\\ \mathbf{G}_2^{(1)} &= \frac{2\pi}{\Lambda_0}\left[\cos\left(\frac{\theta}{2}\right)\hat{x} - \sin\left(\frac{\theta}{2}\right)\hat{y}\right].\end{aligned} \tag{13}$$

The first-order moiré pattern is given by

$$\begin{aligned}\mathbf{G}_{\text{moire}'}^{(1)(2,1)} &= \pm\min[(\mathbf{G}_1^{(2)} + \mathbf{G}_2^{(1)}), (\mathbf{G}_1^{(2)} - \mathbf{G}_2^{(1)})]\\ &= \pm\min[(2\mathbf{G}_1^{(1)} + \mathbf{G}_2^{(1)}), (2\mathbf{G}_1^{(1)} - \mathbf{G}_2^{(1)})]\\ &= \pm\frac{2\pi}{\Lambda_0}\ \min\left[2\cos\left(\frac{\theta}{2}\right)\hat{x}, 2\sin\left(\frac{\theta}{2}\right)\hat{y}\right].\end{aligned} \tag{14}$$

The first term is minimum when $\theta \cong \pi$ and the second term is minimum for $\theta \cong 0$ in which they show additive and subtractive conditions, respectively. The corresponding period of the resulting moiré pattern is $\Lambda_{\text{moire}'} = \frac{\Lambda_0}{2\cos(\frac{\theta}{2})}$ or $\Lambda_{\text{moire}'} = \frac{\Lambda_0}{2\sin(\frac{\theta}{2})}$ for the additive and subtractive cases, respectively, which is equal to the period of the moiré pattern of two similar gratings with the same periods of Λ_0.

Higher-order moiré patterns are given by

$$\begin{aligned}\mathbf{G}_{\text{moire}'}^{(n)(2n,n)} &= \pm\min[(\mathbf{G}_1^{(2n)} + \mathbf{G}_2^{(n)}), (\mathbf{G}_1^{(2n)} - \mathbf{G}_2^{(n)})]\\ &= \pm\min[(2n\mathbf{G}_1^{(1)} + n\mathbf{G}_2^{(1)}), (2n\mathbf{G}_1^{(1)} - n\mathbf{G}_2^{(1)})]\\ &= \pm\frac{2\pi}{\Lambda_0}\ \min\left[2n\cos\left(\frac{\theta}{2}\right)\hat{x}, 2n\sin\left(\frac{\theta}{2}\right)\hat{y}\right],\end{aligned} \tag{15}$$

where it is n times of the fundamental frequency in Eq. (14).

It is worth noting that, in the parallel case where $\theta = 0$ and when $\Lambda_1 = m\Lambda_2$, $m \in \mathbb{N}$, a pseudo-moiré pattern appears (even the gratings have sinusoidal profiles); see Fig. 2 where $\Lambda_1 = 5\Lambda_2$.

B. High-Order Moiré Patterns of Two Linear Gratings Having Relative Fractional Periods

Now, we assume that $3\Lambda_1 = 2\Lambda_2 = 6\Lambda_0$. Therefore, $2|\mathbf{G}_1^{(1)}| = 3|\mathbf{G}_2^{(1)}|$, $m_1 = 2$, and $m_2 = 3$. Similar to the previous example, an angle θ between grids of gratings is considered. The gratings' reciprocal vectors corresponding to their fundamental frequencies are given by

$$\begin{aligned}\mathbf{G}_1^{(1)} &= \frac{2\pi}{2\Lambda_0}\left[\cos\left(\frac{\theta}{2}\right)\hat{x} + \sin\left(\frac{\theta}{2}\right)\hat{y}\right],\\ \mathbf{G}_2^{(1)} &= \frac{2\pi}{3\Lambda_0}\left[\cos\left(\frac{\theta}{2}\right)\hat{x} - \sin\left(\frac{\theta}{2}\right)\hat{y}\right],\end{aligned} \tag{16}$$

and the lowest-order resulting moiré pattern is

$$\begin{aligned}\mathbf{G}_{\text{moire}'}^{(1)(2,3)} &= \pm\min[(\mathbf{G}_1^{(2)} + \mathbf{G}_2^{(3)}), (\mathbf{G}_1^{(2)} - \mathbf{G}_2^{(3)})]\\ &= \pm\min[(2\mathbf{G}_1^{(1)} + 3\mathbf{G}_2^{(1)}), (2\mathbf{G}_1^{(1)} - 3\mathbf{G}_2^{(1)})]\\ &= \pm\frac{2\pi}{\Lambda_0}\ \min\left[2\cos\left(\frac{\theta}{2}\right)\hat{x}, 2\sin\left(\frac{\theta}{2}\right)\hat{y}\right].\end{aligned} \tag{17}$$

Here, similar to Eq. (14), $\theta \cong \pi$ and $\theta \cong 0$ correspond to the additive and subtractive cases, respectively. In addition, the periods of the resulting moiré patterns are $\Lambda_{\text{moire}'} = \frac{\Lambda_0}{2\cos(\frac{\theta}{2})}$ and $\Lambda_{\text{moire}'} = \frac{\Lambda_0}{2\sin(\frac{\theta}{2})}$ for the additive and subtractive cases, respectively. Here, Λ_0 defines the period of the resulting moiré pattern and is given by the *greatest common divisor* of the gratings' periods. In Fig. 3, the above case is illustrated by the resulting patterns of superimposition of two gratings having sinusoidal and binary profiles.

As shown before, higher-orders moiré fringes are given by

$$\begin{aligned}\mathbf{G}_{\text{moire}'}^{(n)(2n,3n)} &= \pm\min[(\mathbf{G}_1^{(2n)} + \mathbf{G}_2^{(3n)}), (\mathbf{G}_1^{(2n)} - \mathbf{G}_2^{(3n)})]\\ &= \pm\min[(2n\mathbf{G}_1^{(1)} + 3n\mathbf{G}_2^{(1)}), (2n\mathbf{G}_1^{(1)} - 3n\mathbf{G}_2^{(1)})]\\ &= \pm\frac{2\pi}{\Lambda_0}\ \min\left[2n\cos\left(\frac{\theta}{2}\right)\hat{x}, 2n\sin\left(\frac{\theta}{2}\right)\hat{y}\right],\end{aligned} \tag{18}$$

where again this frequency is n times of the fundamental frequency in Eq. (17).

In the current case and when $\theta = 0$, pseudo-moiré fringes with a form of equidistant parallel fringes appear with a spacing

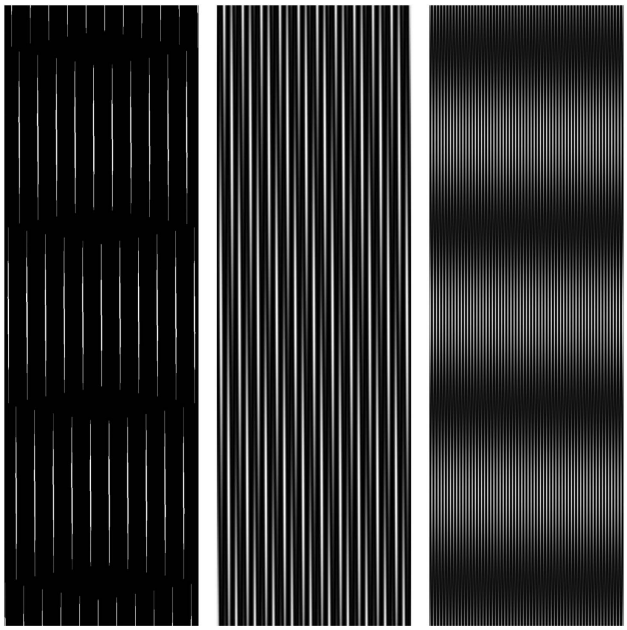

Fig. 3. (a) Superimposition of two binary gratings having periods of $\Lambda_1 = 2\Lambda_0$ and $\Lambda_2 = 3\Lambda_0$ with $\Lambda_0 = 0.4$ mm and a relative rotation angle of 1° between their lines and having the same opening numbers of 0.2; (b) superimposition of the same gratings with sinusoidal profiles; and (c) superimposition of two sinusoidal gratings with equal period Λ_0 and relative rotation angle 1°. Clearly in (b) the moiré pattern does not appear, and in (c) the period of the moiré pattern is the same as (a). The value of $\Lambda_0 = 0.4$ mm is valid when sizes of all patterns are 2.5 cm × 8 cm.

equal $6\Lambda_0$ (*least common multiple* of Λ_1 and Λ_2), as illustrated in Fig. 4.

C. Simultaneous First-Order Moiré Patterns of Different Harmonics of Two Linear Gratings

Here, we examine simultaneous formation of various first-order moiré fringes of two linear gratings having sinusoidal and binary profiles in parallel case. Lines of both of the gratings are in the y direction and the period of one of the gratings is constant, $\Lambda_1 =$ constant, and the period of another one is gradually changed by the x coordinate [see Figs. 5(a)–5(d)]. We consider a reciprocal vector function for the m_2th harmonic of the second grating in the following form:

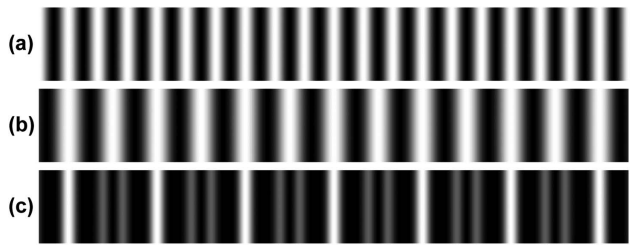

Fig. 4. Linear sinusoidal gratings with (a) $\Lambda_1 = 2\Lambda_0$ and (b) $\Lambda_2 = 3\Lambda_0$. (c) Pseudo-moiré pattern of the gratings in the parallel case.

$$\mathbf{G}_2^{(m_2)} = m_2\left(\frac{2\pi}{\Lambda_2} + \alpha x\right)\hat{x}, \tag{19}$$

where α is a constant that defines the variation rate of the frequency along the x direction. When $\alpha > 0$, it needs $x \geq -\frac{2\pi}{\Lambda_2\alpha}$, and for $\alpha < 0$ the valid range is $x \leq -\frac{2\pi}{\Lambda_2\alpha}$.

First, we consider superimposition of two linear gratings; one has a constant period Λ_1 and both have binary profiles. The frequency of a given first-order moiré pattern produced by the contributions of $\mathbf{G}_1^{(m_1)}$ and $\mathbf{G}_2^{(m_2)}$ can be written as

$$\mathbf{G}_{\text{moire}'}^{(1)(m_1,m_2)}(x) = \pm\left[m_2\left(\frac{2\pi}{\Lambda_2} + \alpha x\right) - m_1\frac{2\pi}{\Lambda_1}\right]\hat{x}, \tag{20}$$

where $m_1, m_2 \in \mathbb{N}$ and the subtractive term is only taken into account. For known values of m_1 and m_2, the corresponding phase function is given by

$$\phi_{\text{moire}'}^{(m_1,m_2)}(x) = \left(\frac{2\pi m_2}{\Lambda_2} - \frac{2\pi m_1}{\Lambda_1}\right)x + \frac{1}{2}m_2\alpha x^2 + \phi_0. \tag{21}$$

From Eq. (20) locations of different moiré fringes can be obtained by

$$x^{(m_1,m_2)} = \frac{2\pi}{\alpha}\left(\frac{m_1}{m_2}\frac{1}{\Lambda_1} - \frac{1}{\Lambda_2}\right), \qquad m_1, m_2 \in \mathbb{N}. \tag{22}$$

When $m_1 = m_2 = 1$ that means only fundamental frequencies of the gratings are contributed in moiré fringes; at the vicinity of position $x_0 = \frac{2\pi}{\alpha}(\frac{1}{\Lambda_1} - \frac{1}{\Lambda_2})$ gratings' periods are the same and parallel first-order moiré fringes appear. When both gratings have sinusoidal profiles, we have only first-order moiré fringes of fundamental harmonics that appear at that position; see Figs. 5(e) and 5(f). For better illustration of the resulting moiré fringes in Fig. 5(f), higher frequency patterns containing gratings structures are removed from the resulting superimposed moiré pattern using Fourier transform and spatial filtering in the frequency domain. This procedure is done on all following resulting moiré patterns.

Now, we consider moiré fringes of higher-order frequencies using Eq. (22). When $\alpha > 0$, over the area $x > x_0$ the fundamental frequency of the second grating increases. Therefore, in the formation of the first-order moiré pattern, the fundamental frequency of the second grating with one of the higher-order frequencies of the first grating is contributed. On the other hand, over the left side area $x < x_0$, as the period of the second grating increases by decreasing x, the fundamental frequency of the first grating and a higher-order frequency of the second grating contribute in the formation of the moiré pattern.

It is possible to get a negative value for α. With this assumption the results change a bit. In summary, according to Eq. (22) we have

$$\begin{aligned} x^{(m_1,m_2=1)} &= \frac{2\pi}{\alpha}\left(\frac{m_1}{\Lambda_1} - \frac{1}{\Lambda_2}\right), \\ x^{(m_1=1,m_2)} &= \frac{2\pi}{\alpha}\left(\frac{1}{m_2\Lambda_1} - \frac{1}{\Lambda_2}\right), \end{aligned} \tag{23}$$

where the first equation refers to the superimposition of a binary grating with a constant period and a sinusoidal linear grating with a gradually varying period, and the next equation

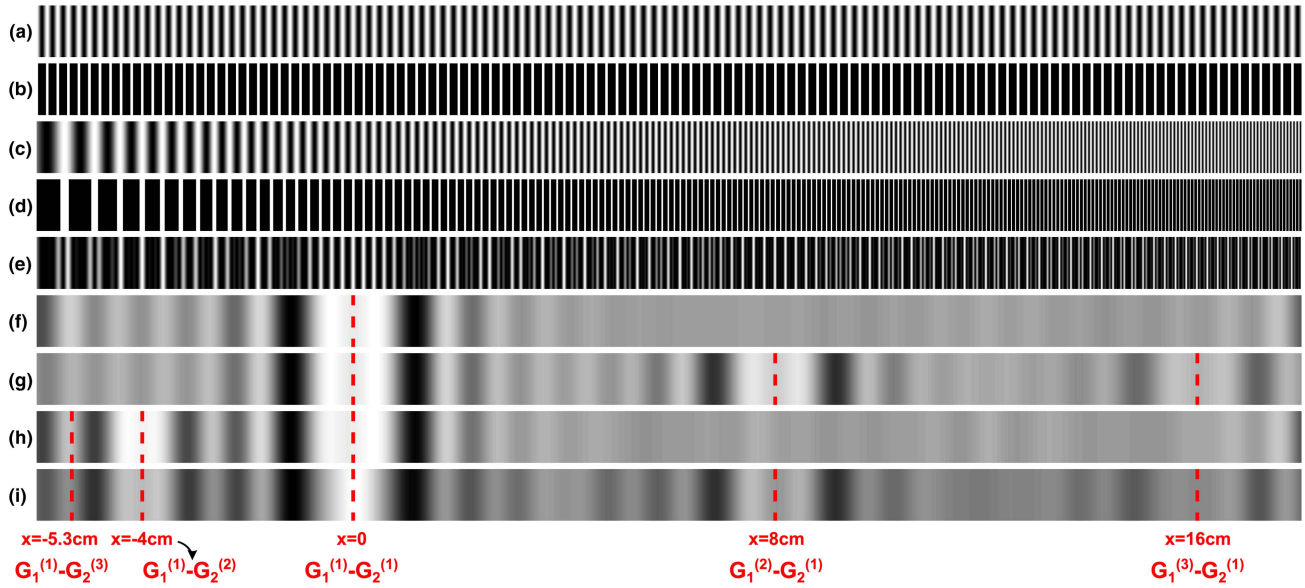

Fig. 5. (a) Linear grating with a sinusoidal profile with $\Lambda_1 = 0.2$ cm. (b) Linear grating with a binary profile with the same period of (a) and an opening number equal to 0.25. (c) Sinusoidal linear grating with a varying spatial frequency with $\Lambda_2 = 0.2$ cm and $\alpha = 3.927$ rad/cm^2. (d) Binary grating with the same periodicity of (c) and an opening number equal to 0.25. (e) Superimposition of the two gratings introduced in (a) and (c). (f) Same pattern of (e) after removing high-frequency patterns. (g) Superimposition of the two gratings introduced in (b) and (c). (h) Superimposition of the two gratings introduced in (a) and (d). (i) Superimposition of the two gratings introduced in (b) and (d). Higher frequencies on moiré patterns were eliminated for more clarity in (f)–(i). All positions of the main moiré fringes are shown with the dashed vertical lines where the resulting main fringes at $x = 8$ cm and $x = 16$ cm have $m_1 = 2$ and $m_1 = 3$, respectively, and at $x = -4$ cm and $x = -5.3$ cm the contributing orders are $m_2 = 2$ and $m_2 = 3$, respectively. The position $x = 0$ relates to $m_1 = m_2 = 1$ in Eq. (23). The values of the above-mentioned length-related parameters are valid when lengths of all shapes are 24 cm.

refers to a binary grating with a varying period and a sinusoidal linear grating.

Other higher-order frequencies of both gratings can be contributed in the formation of moiré patterns where positions of the moiré patterns can be calculated using Eq. (22). In Figs. 5(g)–5(i) several moiré patterns of high-order frequencies are illustrated. As the non-sinusoidal gratings have extra frequencies they naturally produce additional (as compared with sinusoidal) patterns in those areas. In Fig. 5(e), the conventional moiré pattern of the superimposition of two linear gratings having sinusoidal profiles, one with a constant period and another with a variable period, is shown. Figure 5(f) shows the same pattern of Fig. 5(e) after removing the superimposed gratings' high-frequency patterns. A fast Fourier transforming process with the MATLAB software is used for removing the high-frequency patterns (see also [25]) In Fig. 5(g), the moiré patterns of the superimposition of a linear grating having a binary profile and a constant period on a sinusoidal linear grating having variable period are illustrated. Figure 5(h) shows the first-order moiré patterns of different higher-order harmonics of the superimposition of a linear grating having a sinusoidal profile with a constant period on a linear grating with a binary profile and variable period. Figure 5(i) shows the first-order moiré patterns of different higher-order harmonics of the superimposition of two linear gratings having binary profiles in which one has a constant period and another has a varying period.

A similar case of Fig. 5(g) has been previously used for the determination of the pixel size of a monitor [13].

D. Formation of Various First-Order Moiré Patterns in the Superimposition of a Defected Linear Grating and a Defected Fresnel Zone Plate

Here some interesting examples are considered where various superimpositions of a linear grating and a Fresnel zone plate with sinusoidal or binary profiles and consisting of topological defects at different locations are presented. Already in [16] it is shown that when a defected linear grating and a defected Fresnel zone plate having sinusoidal profiles are superimposed, a new zone palate shape appears as the moiré pattern in an area where the linear grating and zone plate have almost equal spatial periods, in which the center of the produced zone plate is taken at that point the gratings have the same periods and their lines are almost parallel. In addition, it is shown that when one of the gratings has a topological defect at that point, the zone plate shape changes to a spiral shape with a topological defect of equal to the same topological defect number of the defected grating. The sign of the defect of the produced pattern may depend on the position of the defect point.

Now we show that when at least one of the superimposed gratings has a binary profile, various first-order moiré patterns simultaneously appear over the superimposed area. Also, it is shown that a dislocated moiré pattern appears when a dislocation is considered for one or both of the gratings over an area where the gratings have almost equal frequency harmonics.

The phase function of a zone plate having a sinusoidal profile and consisting of a defect point with a defect number equal l_1 at position (x_1, y_1) is given by [16]

$$\phi_{\mathrm{ZP}}^{(1)} = \frac{\pi\rho^2}{s} - l_1\varphi_1 + \phi_0, \tag{24}$$

where s is known as the zone plate constant and φ_1 shows the azimuthal angle defined as $\varphi_1 = \arctan(\frac{y-y_1}{x-x_1})$. Here, again, we present m_1th order of the reciprocal vector function as

$$\mathbf{G}_{\mathrm{ZP}}^{(m_1)} = m_1\left(\frac{2\pi\rho}{s}\hat{\rho} - \frac{l_1}{\rho_1}\hat{\varphi}_1\right), \tag{25}$$

where $\hat{\rho}$ is the unit vector corresponding to the radial coordinate in the polar system and $\hat{\varphi}_1$ is the unit vector corresponding to the azimuthal angle φ_1 and ρ_1 is the radial coordinate originated from the (x_1, y_1) point.

The phase function for the fundamental frequency of a defected linear grating with a spatial period and defect number of Λ and l_2 having a sinusoidal profile can be defined as

$$\phi_{\mathrm{DLG}}^{(1)} = \frac{2\pi}{\Lambda}x - l_2\varphi + \phi_0. \tag{26}$$

The grating's defect point is taken at the center of the coordinates system. The m_2th order of the reciprocal vector function is

$$\mathbf{G}_{\mathrm{DLG}}^{(m_2)} = m_2\left(\frac{2\pi}{\Lambda}\hat{x} - \frac{l_2}{\rho}\hat{\varphi}\right), \tag{27}$$

where $\hat{x}$ and $\hat{\varphi}$ are unit vectors corresponding to the x-axis and azimuthal angle, respectively, and ρ is the radial coordinate in the polar system. In Eqs. (26) and (27), both notations of the Cartesian and polar coordinate systems are simultaneously used, for simplicity.

It should be remembered that high-order reciprocal vectors do not exist for the sinusoidal gratings, but for other types of the gratings, for example those having binary profiles, according to Eq. (4), high-order spatial frequencies can be calculated.

In the superimposition of a defected linear grating and a defected zone plate, the reciprocal vector of the resulting moiré pattern using Eqs. (25) and (27) is given by

$$\begin{aligned}\mathbf{G}_{\mathrm{moire}'}^{(1)(m_1,m_2)} &= \pm\min\left[m_1\left(\frac{2\pi\rho}{s}\hat{\rho} - \frac{l_1}{\rho_1}\hat{\varphi}_1\right) \pm m_2\left(\frac{2\pi}{\Lambda}\hat{x} - \frac{l_2}{\rho_2}\hat{\varphi}_2\right)\right] \\ &= \pm\min\left[\left(m_1\frac{2\pi\rho}{s}\hat{\rho} \pm m_2\frac{2\pi}{\Lambda}\hat{x}\right) - \left(\frac{m_1 l_1}{\rho_1}\hat{\varphi}_1 \pm \frac{m_2 l_2}{\rho_2}\hat{\varphi}_2\right)\right],\end{aligned} \tag{28}$$

where $\hat{\varphi}_{1,2}$ and $\rho_{1,2}$ are defined in the coordinates system with the center located at $(x_{1,2}, y_{1,2})$. When $\hat{\rho}$ and $\hat{x}$ are almost parallel, with the minus sign the subtractive term moiré pattern appears and when they are almost antiparallel, with the plus sign the additive term moiré pattern appears. The additive and subtractive moiré patterns appear at the vicinity of $x = \mp\frac{m_2 s}{m_1\Lambda}$, respectively. Now we consider a general case in which both of the gratings consist of some topological defects with the given values of defect numbers at places in which the fundamental or higher-order frequencies of the gratings are equal. At the vicinity of a point that two gratings have the same frequency components of $m_1\mathbf{G}_2$ and $\pm m_2\mathbf{G}_2$, and the gratings

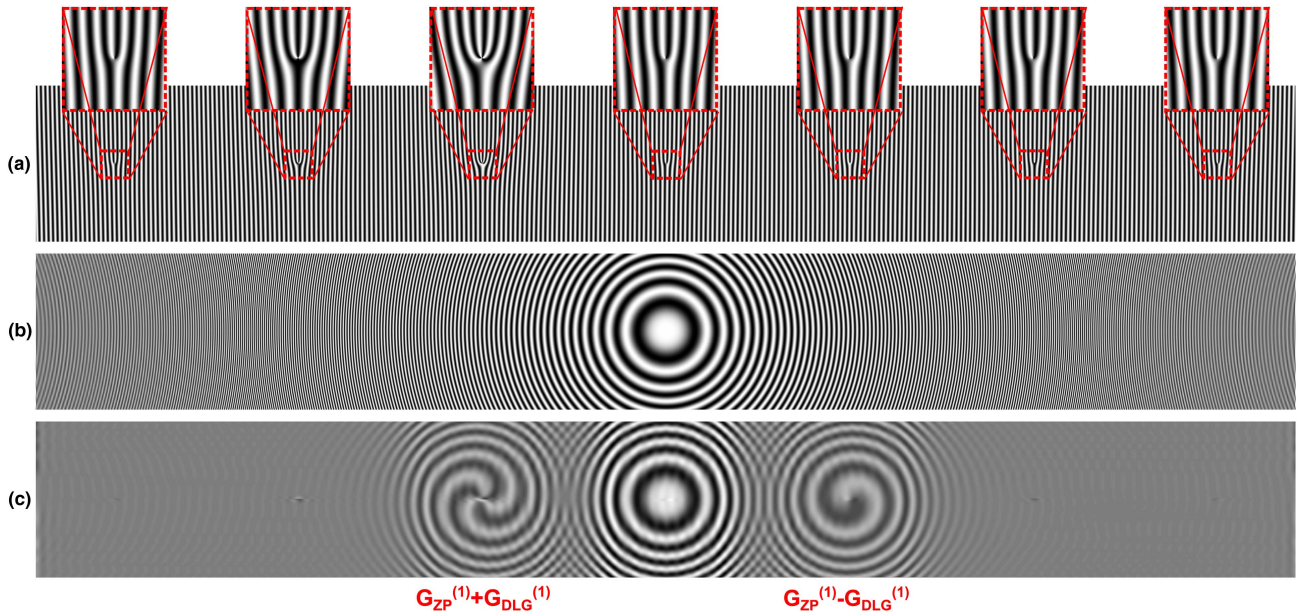

Fig. 6. (a) Defected linear grating with a sinusoidal profile and a period of $\Lambda = 0.857$ cm. The grating has seven defect points with defect numbers of $l_2 = +1$ chosen at $x = 0$, $+3.5$ cm, $+7$ cm, $+10.5$ cm, and $x = -10.5$ cm points and with a defect number of $l_2 = +3$ locates at $x = -3.5$ cm and with a defect number of $l_2 = +2$ locates at $x = -7$ cm. The locations of all the defect points are determined by the red squares and the structure of the grating is enlarged by suitable insets at those points. (b) A Fresnel zone plate with a sinusoidal profile and $s = 0.3$ cm^2. (c) Superimposition of the introduced structures in (a) and (b) where higher spatial frequencies are eliminated. In (c), as the central pattern is the initial pattern of the zone plate, it is not manipulated by the defect of the linear grating. At the right side, the subtractive term moiré pattern appears around $x = +3.5$ cm with a defect number of -1, and at the left side, around $x = -3.5$ cm the additive term moiré pattern appears with a defect number of $+3$. The values of the above-mentioned length parameters are valid when the sizes of all subfigures are 24 cm × 3 cm.

defect numbers are l_1 and l_2, using Eq. (28) the defect number of the resulting moiré pattern can be written as

$$l_{\text{moire}'} = (m_1 l_1 \pm m_2 l_2), \tag{29}$$

where the plus sign corresponds to the additive term moiré pattern and the minus sign shows the subtractive term moiré pattern.

Now we consider some different cases. When both of the gratings have sinusoidal profiles, $|m_1|, |m_2| = 0, 1$, additive and subtractive term moiré patterns are resulted by the first-order harmonics of the gratings. The resulting patterns have zone plate shapes with a zone plate constant of s and centers located at $x = \mp \frac{s}{\Lambda}$. Now consider that the linear grating consists of some topological defects in which two of them are located at places where both of the gratings have the same fundamental frequencies. At the vicinity of these points, as is apparent from Fig. 6, the resulting moiré patterns appear as spiral zone plates. Each of the moiré patterns has the same defect number as the linear grating at the corresponding point, $l_{\text{moire}'} = \pm l_2$, where plus is for the left side pattern and minus is for the right side pattern.

In Fig. 7(a) a linear grating with a binary profile consisting of some defects at different points is illustrated. The defect points or dislocations are selected over areas in which the gratings have almost equal frequency harmonics. In Fig. 7(b) a Fresnel zone plate with a sinusoidal profile is shown. In Fig. 7(c) instantaneously resulting moiré patterns of the first- and higher-order frequencies of the linear grating and first-order frequency of the Fresnel zone plate at different positions are shown. The defected points of the linear grating are chosen at places in which the contributed frequencies of the gratings at those points are equal. As is apparent from Fig. 7(c), other spiral zone plate patterns simultaneously appear over the superimposed area in which the centers of the patterns are located at $x = \mp \frac{m_2 s}{\Lambda}$ with a defect number of $l_{\text{moire}'} = \pm m_2 l_2$.

In Figs. 8–10 various cases of the superimposition of a zone plate with a binary profile on a linear grating with a sinusoidal profile are presented. Again, the defect points of the gratings are selected over areas in which the gratings have almost equal frequency harmonics. In Fig. 8 the linear grating has some defect points. In Fig. 9 the zone plate consists of some defect points. In Fig. 10 both of the superimposed structures have some defect points at locations in which their spatial frequencies or their higher harmonics are equal.

We see that, in the superimposition of a defected Fresnel zone plate having a binary profile and a defected linear grating with a sinusoidal profile, additional spiral patterns appear at the vicinity of the central spiral zone plate pattern, $x = \mp \frac{s}{m_1 \Lambda}$, with the topological defects equal $m_1 l_1 \pm l_2$ (see Figs. 8–10).

It should be noted that in the view of Figs. 5–10 through an LCD screen or over a printed page with a low dots per inch, sometimes unwanted moiré fringes appear at different locations that differ from the main moiré fringes discussed in the paper.

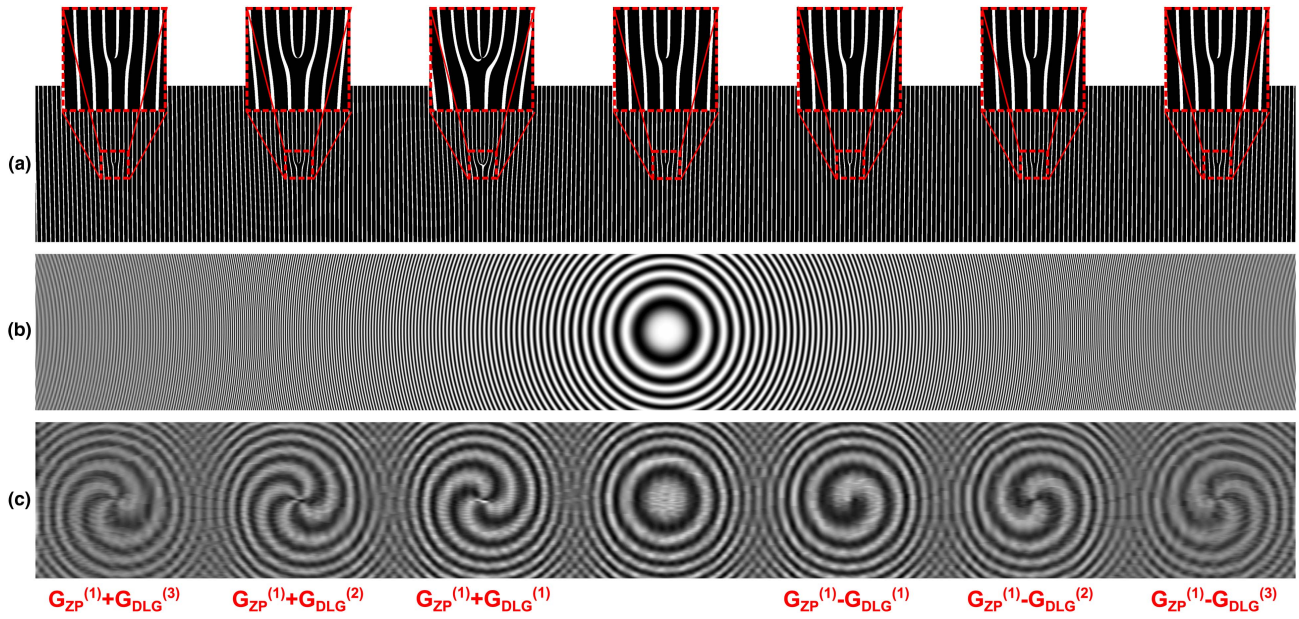

Fig. 7. (a) Defected linear grating with a binary profile and an opening number of 0.2 and a period of $\Lambda = 0.857$ cm. The linear grating has seven defect points with defect numbers of $l_2 = +1$ chosen at $x = 0$, + 3.5 cm, + 7 cm, + 10.5 cm, and $x = -10.5$ cm points and with a defect number of $l_2 = +3$ at $x = -3.5$ cm and with a defect number of $l_2 = +2$ at $x = -7$ cm. The locations of all defect points are determined by the red squares and the structure of the grating is enlarged by suitable insets at those points. (b) Fresnel zone plate with a sinusoidal profile and $s = 0.3$ cm^2. (c) Superimposition of the gratings presented in (a) and (b). In (c), six moiré patterns of different pairs of frequencies of the gratings are shown. They simultaneously appear at $x = +3.5$ cm, $x = +7$ cm, and $x = +10.5$ cm with defect numbers of −1, −2, and −3, respectively, and at $x = -3.5$ cm, $x = -7$ cm, and $x = -10.5$ cm with defect numbers of +3, +4, and +3, respectively. Here, again, the central zone plate shows the main pattern of the Fresnel zone plate and is not a moiré pattern. Therefore, it cannot reflect the dislocation of the defected grating. For the subtractive term moiré patterns on the right side, the defect numbers are $l_{\text{moire}'} = (m_1 l_1 - m_2 l_2)$, and for the additive term moiré patterns on the left side, the defect numbers are $l_{\text{moire}'} = (m_1 l_1 + m_2 l_2)$, where m_1 and m_2 are the contributed frequency orders of the defected linear and Fresnel gratings, respectively (here, $m_1 = 1$ and $m_2 = 1, 2, 3$). The values of the above-mentioned length-related parameters are valid when the sizes of all subfigures are 24 cm × 3 cm.

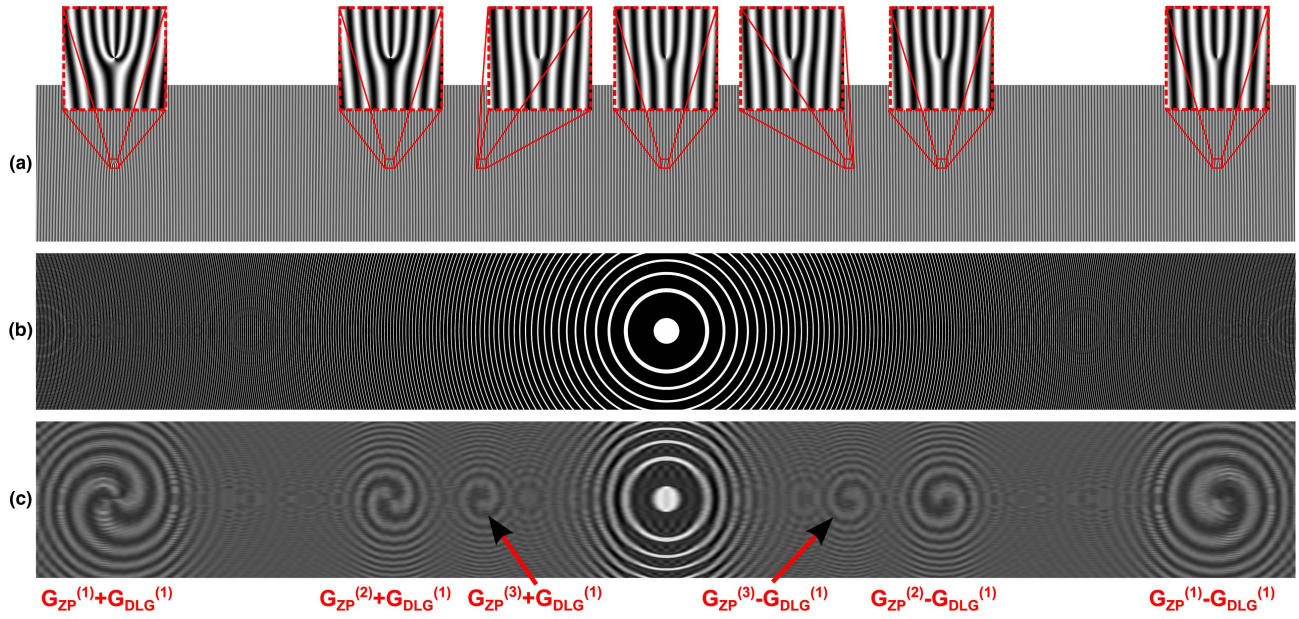

Fig. 8. (a) Defected linear grating with a sinusoidal profile and a period of $\Lambda = 0.286$ cm. The linear grating consists of seven defect points with defect numbers of $l_2 = +1$ chosen at $x = 0$, $+3.5$ cm, $+5.25$ cm, $+10.5$ cm, and $x = -3.5$ cm points and with a defect number of $l_2 = +3$ at $x = -10.5$ cm and a defect number of $l_2 = +2$ at $x = -5.25$ cm. (b) A Fresnel zone plate with a binary profile and an opening number equal to 0.2, and $s = 0.3$ cm^2. (c) Superimposition of gratings introduced in (a) and (b) where, here again, higher spatial frequencies are eliminated. As is apparent from (c), at least six spiral-like patterns appear at $x = +10.5$ cm, $+5.25$ cm, and $+3.5$ cm with the same topological defects of -1 and for the point selected at $x = -10.5$ cm with a topological defect of $+3$, at -5.25 cm with a defect number of $+2$, and at -3.5 cm with a defect number of $+1$. Using $m_2 = 1$ and $m_1 = 1, 2, 3$ in $l_{\text{moire}'} = (m_1 l_1 \pm m_2 l_2)$ topological defects of the moiré pattern can be determined. The values of length-related parameters are valid when the sizes of all subfigures are 24 cm × 3 cm.

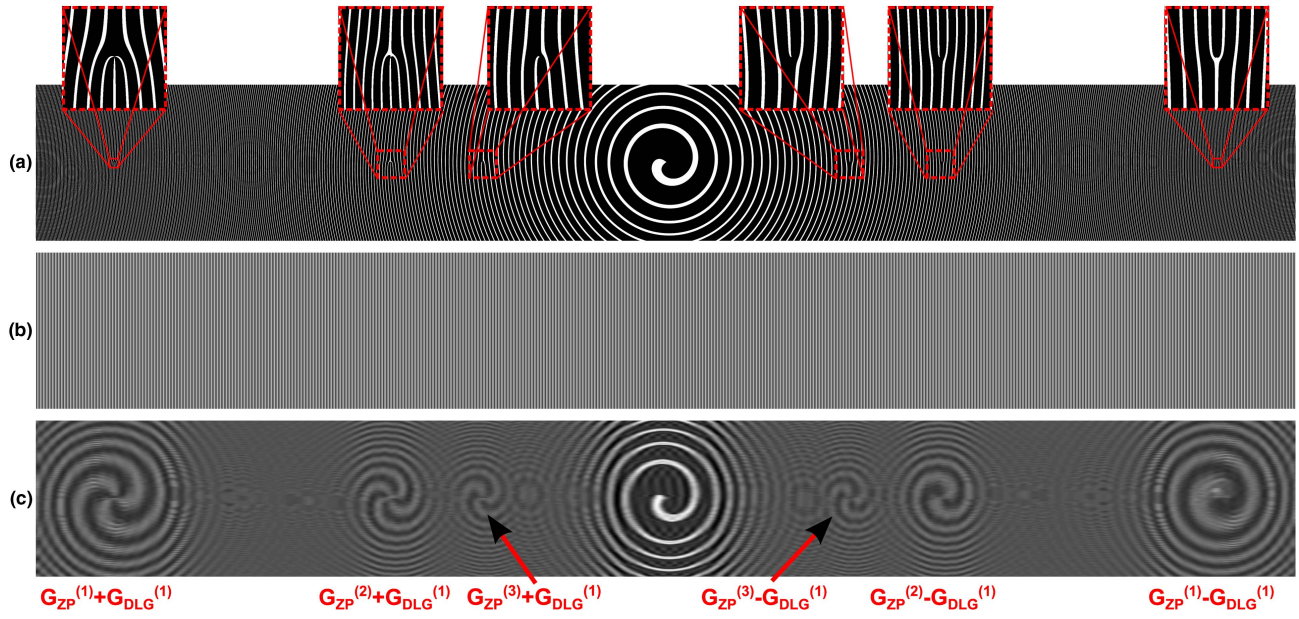

Fig. 9. (a) Defected Fresnel zone plate with a binary profile and an opening number equal to 0.2, and $s = 0.3$ cm^2, where seven defect points with defect numbers of $l_1 = +1$ chosen at $x = 0$, $+3.5$ cm, $+5.25$ cm, $+10.5$ cm, and $x = -3.5$ cm points and with a defect number of $l_1 = +2$ at $x = -5.25$ cm and with a defect number of $l_1 = +3$ at $x = -10.5$ cm. (b) A linear grating with a sinusoidal profile and a period of $\Lambda = 0.286$ cm. (c) Superimposition of the presented gratings in (a) and (b). As is seen in (c), at least six spiral-like patterns appear with topological defects equal to $+3$ at $x = +3.5$ cm, equal to $+2$ at $+5.25$ cm, equal to $+1$ at $+10.5$ cm, equal to $+3$ at $x = -3.5$ cm, equal to $+4$ at $x = -5.25$ cm, and equal to $+3$ at $x = -10.5$ cm. Again, the central spiral pattern is not a moiré pattern and shows only the main pattern of the Fresnel zone plate. The values of the above-mentioned length-related parameters are valid when the sizes of all subfigures are 24 cm × 3 cm.

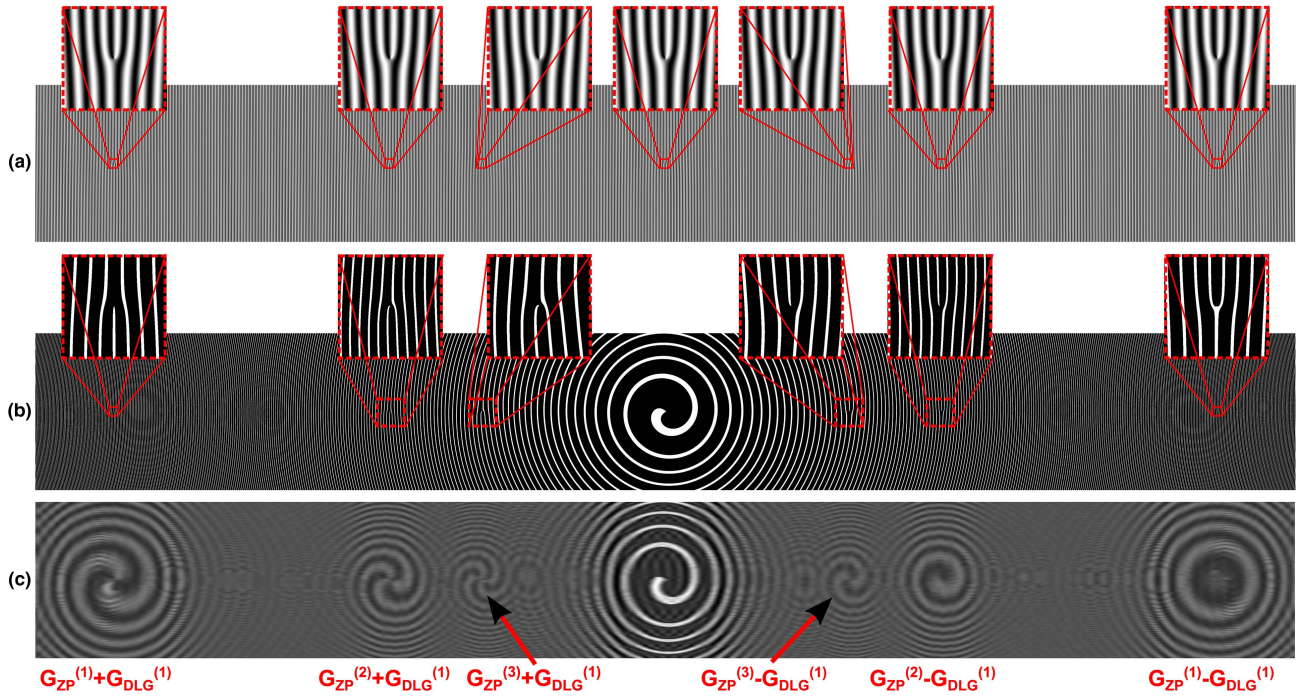

Fig. 10. (a) Defected linear grating with a sinusoidal profile and a period of $\Lambda = 0.286$ cm consisting of seven defect points with the same amount of defect numbers $l = 1$ selected at 0, $\pm$ 3.5 cm, $\pm$ 5.25 cm, $\pm$ 10.5 cm. (b) Fresnel zone plate with a binary profile and an opening number equal to 0.2, and $s = 0.3$ cm^2. It consists of seven defect points with the same amount of defect numbers $l = 1$ selected at 0, $\pm$ 3.5 cm, $\pm$ 5.25 cm, $\pm$ 10.5 cm. (c) Superimposition of defected linear grating presented in (a), and defected Fresnel zone plate presented in (b). As is seen in (c), at least six new spiral-like patterns appear with topological defects equal to +2 at $x = +3.5$ cm, equal to +1 at +5.25 cm, equal to 0 at +10.5 cm, equal to +4 at $x = -3.5$ cm, equal to +3 at $x = -5.25$ cm, and equal to +2 at $x = -10.5$ cm. Using $m_2 = 1$ and $m_1 = 1, 2, 3$ in $l_{\text{moire}'} = (m_1 l_1 \pm m_2 l_2)$ topological defects of the moiré pattern can be determined. The values of the above-mentioned length-related parameters are valid when the sizes of all subfigures are 24 cm × 3 cm.

5. CONCLUSION

A simple and comprehensive approach was presented for the moiré fringes formulation, and moiré fringes of combinational frequencies were classified into four classes: the conventional moiré pattern, moiré fringes of higher-order harmonics, higher-order moiré patterns, and pseudo-moiré patterns. The reciprocal vectors approach was used in distinction of the higher-order moiré patterns from the first-order moiré fringes of higher-order harmonics. We determined the general conditions for simultaneous formation of first-order moiré patterns of different pairs of higher-order frequencies. By the aid of some typical examples based on computational simulations, a detailed development of the proposal was presented. It is shown that in the superimposition of two gratings in which at least one has a varying period and another has a non-sinusoidal profile, simultaneous first-order moiré patterns are formed at different zones of the superimposed area. As a special case, superimposition of a liner grating and a Fresnel zone plate was investigated with more details when one or both of gratings have binary profiles and consist of some topological defects at the areas that two gratings have the same frequency components. We showed that a given dislocation of the superimposed gratings appears as a dislocation on the resulting moiré pattern and the moiré pattern's defect number multiplied by the order of contributed combinational frequencies.

The presented approach can be used for interpreting the daily-life-observed simultaneously formed first-order moiré patterns, such as different moiré patterns observed on an image of an escalator grabbed by a digital camera or the same patterns appearing on the image of a fence recorded with a skew angle. By analyzing the resulting moiré patterns one can specify the corresponding imaging systems, periodic structures, and geometry of the respective imaging setups.

Funding. Institute for Advanced Studies in Basic Sciences (IASBS) (G2018IASBS12632); Iran National Science Foundation (INSF) (95001286).

†These authors contributed equally to this work.

REFERENCES

1. V. Ronchi, "Forty years of history of a grating interferometer," Appl. Opt. **3**, 437–451 (1964).
2. P. S. Theocaris, "Moiré fringes: a powerful measuring device," Appl. Mech. Rev. **15**, 333–339 (1962).
3. K. Patorski, S. Yokozeki, and T. Suzuki, "Moiré profile prediction by using Fourier series formalism," Jpn. J. Appl. Phys. **15**, 443–456 (1976).
4. G. Indebetouw and R. Czarnek, *Selected Papers on Optical Moiré and Applications*, Society of Photo Optical (1992), Vol. **64**.
5. G. Oster, M. Wasserman, and C. Zwerling, "Theoretical interpretation of moiré patterns," J. Opt. Soc. Am. **54**, 169–175 (1964).

6. K. Patorski, *Handbook of the Moiré Fringe Technique* (Elsevier Science, 1993).
7. I. Amidror, *The Theory of the Moiré Phenomenon*, Aperiodic Layers (Springer Netherlands, 2007), Vol. **II**.
8. M. Abolhassani and M. Mirzaei, "Unification of formulation of moiré fringe spacing in parametric equation and Fourier analysis methods," Appl. Opt. **46**, 7924–7926 (2007).
9. I. Amidror, *The Theory of the Moiré Phenomenon*, Periodic Layers (Springer-Verlag, 2009), Vol. **I**.
10. H. D. Polster, J. Pastor, R. M. Scott, R. Crane, P. H. Langenbeck, R. Pilston, and G. Steinberg, "New developments in interferometry," Appl. Opt. **8**, 521–556 (1969).
11. K. Patorski, M. Wielgus, M. Ekielski, and P. Kazmierczak, "AFM nanomoiré technique with phase multiplication," Meas. Sci. Technol. **24**, 035402 (2013).
12. O. Bryngdahl, "Moiré and higher grating harmonics," J. Opt. Soc. Am. **65**, 685–694 (1975).
13. M. R. Abolhassani, "Pixel size determination of a monitor using moiré fringe," Opt. Eng. **49**, 033608 (2010).
14. A. B. Naden, K. J. O'Shea, and D. A. MacLaren, "Evaluation of crystallographic strain, rotation and defects in functional oxides by the moiré effect in scanning transmission electron microscopy," Nanotechnology **29**, 165704 (2018).
15. S. Rasouli and M. Tavassoly, "Analysis of the moiré pattern of moving periodic structures using reciprocal vector approach," J. Phys. Conf. Ser. **350**, 012032 (2012).
16. S. Rasouli and M. Yeganeh, "Formulation of the moiré patterns formed by superimposing of gratings consisting topological defects: moiré technique as a tool in singular optics detections," J. Opt. **17**, 105604 (2015).
17. M. Yeganeh and S. Rasouli, "Investigation of the moiré patterns of defected radial and circular gratings using the reciprocal vectors approach," J. Opt. Soc. Am. A **33**, 416–425 (2016).
18. S. Rasouli and M. Yeganeh, "Moiré patterns of curved line quasi-periodic structures," J. Opt. Soc. Am. A **34**, 1746–1756 (2017).
19. S. Rasouli and D. Hebri, "Contrast enhanced quarter-Talbot images," J. Opt. Soc. Am. A **34**, 2145–2156 (2017).
20. I. Amidror and R. D. Hersch, "The role of Fourier theory and of modulation in the prediction of visible moiré effects," J. Mod. Opt. **56**, 1103–1118 (2009).
21. Y. Kim, G. Park, J. Jung, J. Kim, and B. Lee, "Color moiré pattern simulation and analysis in three-dimensional integral imaging for finding the moiré–reduced tilted angle of a lens array," Appl. Opt. **48**, 2178–2187 (2009).
22. V. Saveljev and S. Kim, "Experimental observation of moiré angles in parallax barrier 3D displays," Opt. Express **22**, 17147–17157 (2014).
23. L. Kong, S. Cai, Z. Li, G. Jin, S. Huang, K. Xu, and T. Wang, "Interpretation of moiré phenomenon in the image domain," Opt. Express **19**, 18399–18409 (2011).
24. K. Patorski, K. Pokorski, and M. Trusiak, "Fourier domain interpretation of real and pseudo-moiré phenomena," Opt. Express **19**, 26065–26078 (2011).
25. S. Rasouli and M. T. Tavassoly, "Application of moiré technique to the measurement of the atmospheric turbulence parameters related to the angle of arrival fluctuations," Opt. Lett. **31**, 3276–3278 (2006).